Article

Comparison of Micro-Mixing in Time Pulsed Newtonian Fluid and Viscoelastic Fluid

Meng Zhang [1,2,*,†], Wu Zhang [2,3,†], Zhengwei Wu [4], Yinan Shen [2], Yicheng Chen [1], Chaofeng Lan [1], Fengchen Li [1] and Weihua Cai [1,*]

[1] School of Energy Science and Engineering, Harbin Institute of Technology, Harbin 150001, China; cychit@163.com (Y.C.); lanchaofengl@126.com (C.L.); lifch@hit.edu.cn (F.L.)
[2] School of Engineering and Applied Sciences, Harvard University, Cambridge, MA 02138, USA; zh0002wu@outook.com (W.Z.); yinanshen@g.harvard.edu (Y.S.)
[3] School of Physics and Electronics, Guangzhou University, Guangzhou 510000, China
[4] Department of Biomedical Engineering and Biotechnology, University of Massachusetts Lowell, Lowell, MA 01854, USA; zhengwei_wu@student.uml.edu
[*] Correspondence: meng.zhang_china@outlook.com (M.Z.); caiwh@hit.edu.cn (W.C.)
[†] These authors contributed equally to this work.

Abstract: Fluid mixing plays an essential role in many microfluidic applications. Here, we compare the mixing in time pulsing flows for both a Newtonian fluid and a viscoelastic fluid at different pulsing frequencies. In general, the mixing degree in the viscoelastic fluid is higher than that in the Newtonian fluid. Particularly, the mixing in Newtonian fluid with time pulsing is decreased when the Reynolds number Re is between 0.002 and 0.01, while it is enhanced when Re is between 0.1 and 0.2 compared with that at a constant flow rate. In the viscoelastic fluid, on the other hand, the time pulsing does not change the mixing degree when the Weissenberg number $Wi \leq 20$, while a larger mixing degree is realized at a higher pulsing frequency when $Wi = 50$.

Keywords: microfluidic mixing; pulsed flow; viscoelastic fluid; Newtonian fluid

1. Introduction

In the swift development of the micro-fabrication process, microfluidic technology has been widely recognized in many practical applications such as medical diagnostics [1], biological analysis [2, 3], chemical analysis [4–6], and heat and mass transfer [7,8], etc. In these applications, reagent mixing is usually a critical process, which largely affects the efficiency and performance of the work. Conventionally, a good and fast mixing relies on the chaotic and turbulent flow instabilities of the fluid and requires a huge Reynolds number of the flow [8–11]. However, in the microfluidic mixer, the large Reynolds number is impeded due to the micro-scaled structural dimensions, and the fluid is usually confined as laminar flow. As a result, the mixing mostly relies on the diffusion, which requires long flow distance and is very inefficient.

Various approaches have been developed to improve the microfluidic mixing, and are usually categorized into active methods and passive methods [12–14]. For passive methods, the microchannel configurations are optimized to increase the reagent contact area or contact time. This is usually based on the fluid lamination or the chaotic advection [15,16]. In a multi-lamination mixer, four inlets were used to reduce the thickness of the fluid layer, and a throughput of 30 μL/min was achieved [17]. Another passive mixer improved the efficiency by rotation, splitting and recombination of the fluids in the microchannel system, in which the interfacial area between two fluids was increased by many times [18]. A chaotic advection-based microfluidic mixer usually increases the efficiency by splitting,

stretching, folding and breaking up the fluids [12]. Such a mixer usually requires a 3-dimensional (3D) structure. For example, a 3D mixer consisting of capillaries with different angles was developed, and the mixing efficiency was improved even with a small pressure drop [19]. A mixer with 3D V-shaped channels and triangular chambers was also designed which realized a mixing efficiency as high as 90% at *Re* less than 150 [20]. In contrast to the passive mixer, the active mixer relies on the external fields to stir the fluid and improve the mixing efficiency. Different external excitations are proposed such as acoustic waves [21], ultrasonics [22], electro-hydrodynamics [23,24] and magnetohydrodynamic pumping [25].

Besides the reliance on external fields, the flow is also controlled by introducing time pulsing to the flow [26–28]. Utilizing the time pulsing, less energy is consumed compared with the active method, and the mixer configuration can be simplified greatly compared with that in the passive method. For example, the structure of "├", "Y", and "T" shape have been reported to improve the mixing efficiency by mechanically pumping two reagents in a sinusoidal, periodic fashion [29,30]. Aperiodic perturbation flows were also studied for the improvement of mixing in the microfluidic channel [31].

Despite the fact that much research has focused on the time pulsing mixing, this study mainly concentrates on the mixing in a Newtonian fluid. In fact, the rheological properties of the fluid also have a high impact on the mixing efficiency. Recently, viscoelastic fluid is proposed to improve the mixing efficiency in the passive microfluidic channels [32–34].

In the viscoelastic fluid, elastic stress only decays after a characteristic time due to its elasticity. For its viscoelastic nature, the viscoelastic fluid can realize chaotic vortices even at a low Reynolds number condition [34,35]. In this paper, by applying the pulsing time approach, we experimentally compared the viscoelastic fluid mixing with the Newtonian fluid mixing in a T-junction microfluidic channel. A time pulsing with square wave modulation is applied to the flow, and the impact of the pulsing frequency and the flow rate on the mixing are investigated for both fluids.

2. Materials and Methods

2.1. Micro-Mixer Design and Fabrication

The T-junction microfluidic mixer is designed as shown in Figure 1a. Fluids of the same type are injected into two inlets I_A and I_B of the T-junction. The fluid on one side contains a small amount of fluorescent dye for experimental view. The two fluids are confluent at the center of the inlet channel and flow into a narrow channel before finally entering into an expanded mixing channel. The fluorescent color in the mixing channel is monitored to determine the mixing efficiency at the flow distance, S_0, from the inlet channel. The length and width of the inlet channels are $L_1 = 2$ mm and $W_1 = 100$ μm, respectively. The confluence channel has dimensions of $L_2 = 600$ μm and $W_2 = 50$ μm, and the mixing channel has dimensions of $L_3 = 2$ mm and $W_3 = 600$ μm. The mixer structure has a depth of $h = 100$ μm, and the outlet is set at the end of the mixing channel.

The T-junction is fabricated using standard soft lithography processes. The mold of the design is first fabricated by spinning coat, exposure and development of a 100 μm thick SU8 photoresist on a silicon wafer. Then, the liquid polydimethylsiloxane (PDMS) consisting of pre-polymer (base) and cross-linker (curing agent) with a weight ratio of 10:1 is poured onto the SU8 mold. The PDMS becomes solid after 4 h of heating in the 65 °C oven. The solid PDMS with the mixer pattern is bonded to a glass slide after plasma treatment, and the microfluidic channel is formed. The completed T-junction mixer chip is shown in Figure 1b.
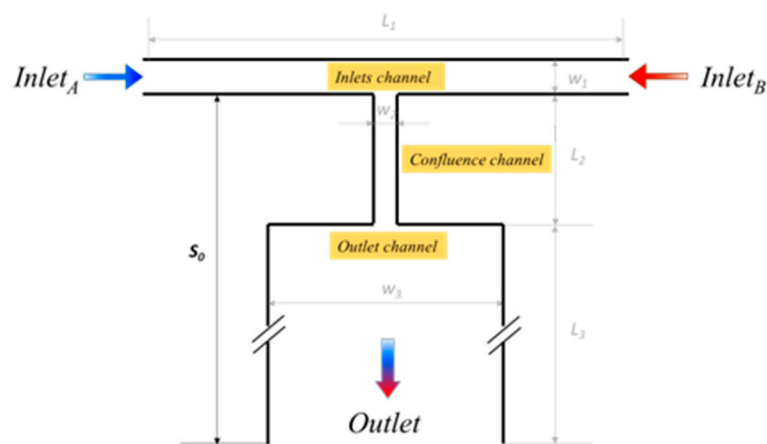
(**a**)
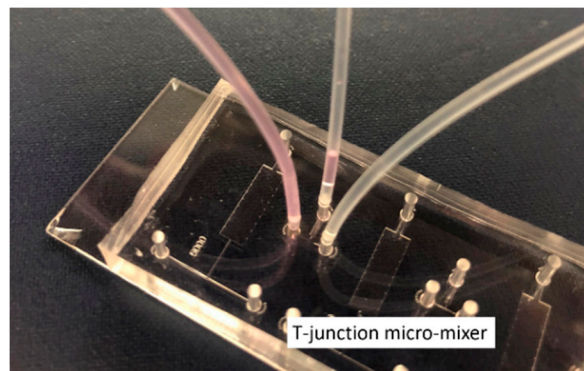
(**b**)

Figure 1. (**a**) The design and (**b**) the fabricated chip of the T-junction microfluidic mixer.

2.2. Materials and Underlying Physics

In the experiment, we studied both the Newtonian fluid mixing and viscoelastic fluid mixing. In the Newtonian fluid, the response of a simple shear has a linear relationship between the applied shear stress and the rate of shear, i.e., $\sigma_{yx} = \eta \dot{\gamma}_{yx}$, where σ_{yx} is the shear stress, $\dot{\gamma}_{yx}$ is the shear rate and η is the viscosity value of the fluid. The relative balance between the inertial and viscous forces are normally characterized with the dimensionless Reynolds number, defined as $Re = \rho UL/\eta$, where L is the characteristic length of the channel, U is the flow rate in the channel and ρ is the density of the fluid. In the microfluidic channel, the Re number is usually smaller than 100, and often smaller than 1 due to the reduced length scale of the channel. The viscous force is dominant to the inertial force and the fluid is usually laminar. So the mixing only depends on the molecular diffusion [36].

The viscoelastic fluid usually contains polymer chains, which can be stretched by the stress from the fluid and relax to an equilibrium state when the stress is released. Therefore, significant elasticity is manifested, and the flow behaviors are enriched. The elasticity can be characterized using the Weissenberg number, defined as $Wi = \lambda U/L$, where λ is the relaxation time, referring to the characteristic stretch-relax time of the polymer. Wi qualifies the nonlinear response of the fluid. The onset of elastic instabilities at high Wi is a hallmark of viscoelastic fluid, even under creeping flows [37]. Such instabilities were experimentally observed in a number of flow geometries, such as Taylor–Couette, contraction and lid-driven cavity flows, etc [38–40]. Currently, it is widely accepted that the instability is related to streamline curvature, which generates tensions along streamlines, leading to flow destabilization [36].

Here, the expanded T-junction mixer introduces the stress to the polymer in the viscoelastic fluid. For the mixing comparison, the Newtonian fluid, 75% glycerol is used, which has a viscosity of 25 mPa·s. For the viscoelastic fluid, 100 ppm polyacrylamide (PAM) with a molecular weight of 18 million is used, which has a similar viscosity (27 mPa·s) with that of glycerol at the shear rate of 100 1/s and relaxation time λ of about 0.12 s.

2.3. Experimental Setup

In the mixing analysis, the same types of fluids are injected from the two inlets of the T-junction mixer, which are named fluid A and fluid B, respectively. Rhodamine B is diluted in fluid A as fluorescent dye with a concentration of 10 μg/mL. The dye is excited by a 475 nm laser, and the fluorescent color in the channel is recorded as the grey value C_i at every pixel i. The grey value depends on the dye concentration and can be used to derive the mixing efficiency. The flow rate Q is modulated by a time pulsing signal with a square wave function at I_A while at I_B, it is a constant. The flow rates are expressed as:

$$Q_1(t) = Q_0\{1 + sgn[sin(2\pi f t)]\} \tag{1a}$$

$$Q_2 = Q_0 \tag{1b}$$

where Q_0 is the flow rate amplitude and f is the time pulsing frequency. The flow rate at I_A oscillates between 0 and $2Q_0$ with a period of $1/f$ and a duty cycle of 50%. The time pulsing signal will disturb the flow and further affect the mixing between fluid A and fluid B.

2.4. Mixing Degree Characterization

As the injected flow rate is time-dependent, both the instantaneous mixing degree MD_t and timely averaged mixing degree $\overline{MD}$ are characterized. The MD_t for the cross line with a distance S_0 from the inlet channel at a specific recorded time t_j is expressed as:

$$MD_t = 1 - \sqrt{\sum_{i=1}^{P} \frac{\left(\frac{C_i}{C_0} - 1\right)^2}{P}} \tag{2}$$

where C_i is the recorded grey value at the pixel i on the cross line of the channel with the total pixel number of P. C_0 is the mean value of the recorded grey values within the mixing channel. It can be seen that $MD_t = 1$ for the full mixing case while $MD_t = 0$ for the no mixing case. MD_t presents the instantaneous mixing degree. To derive the average mixing degree $\overline{MD}$, we consider the fluid flowing through the cross line S_0 in an adequately long recorded time range t_0 as a collection of the fluid flowing through S_0 at every recorded time t_i. Therefore, the averaged mixing degree can be expressed as:

$$\overline{MD} = 1 - \sqrt{\sum_{j=1}^{N} \frac{\left(MD_{t=t_j} - 1\right)^2}{N}} \tag{3}$$

where N is the number of recorded frames for the concentration profile. We can also see that $\overline{MD} = 1$ when the fluid is fully mixed at every instantaneous time, while $\overline{MD} = 0$ when there is no mix at every instantaneous time.

3. Results and Discussion

3.1. Mixing in the Newtonian Fluid

We first investigate the mixing in the T-junction mixer when glycerol is injected into both inlets at the same constant flow rate. The fluorescent concentration profile in the mixing channel is illustrated in Figure 2a as Q_0 varies from 10 μL/h to 1000 μL/h. The corresponding Reynolds number *Re* ranges

from 0.002 to 0.2. The color in the flow map indicates the normalized concentration profile of the fluorescent dye. The red color presents a fluorescent dye concentration close to 1, while the blue color presents a concentration close to 0. At $Q_0 = 10$ μL/h, there is a wide green regime at the center of the channel, indicating good mixing between fluid A and the fluid B. As the flow rate increases to 50 μL/h and to 100 μL/h, the green regime largely shrinks and the mixing degree is lowered. We quantitatively characterize the mixing using the time-averaged mixing degree $\overline{MD}$ as expressed in Equation (3). $\overline{MD}$ is derived for the line across the mixing channel with a distance S_0 from the inlet channel. Here, we derive the $\overline{MD}$ starting at distance $S_1 = 1000$ μm and ending at a distance $S_2 = 2000$ μm from the inlet channel, as shown in Figure 2b. As Q_0 increases from 10 μL/h (black line) to 50 μL/h (red line) and to 100 μL/h (green line), $\overline{MD}$ is greatly decreased in the observed area. The significant mixing decrease in the low flow rate regime stems from the diffusion time decrease when the flow rate increases. However, as the flow rate changes from 200 μL/h to 1000 μL/h, the decrease in $\overline{MD}$ is quite small. This indicates that the impact of the intrinsic diffusion on the mixing becomes weak in the high flow rate regime.
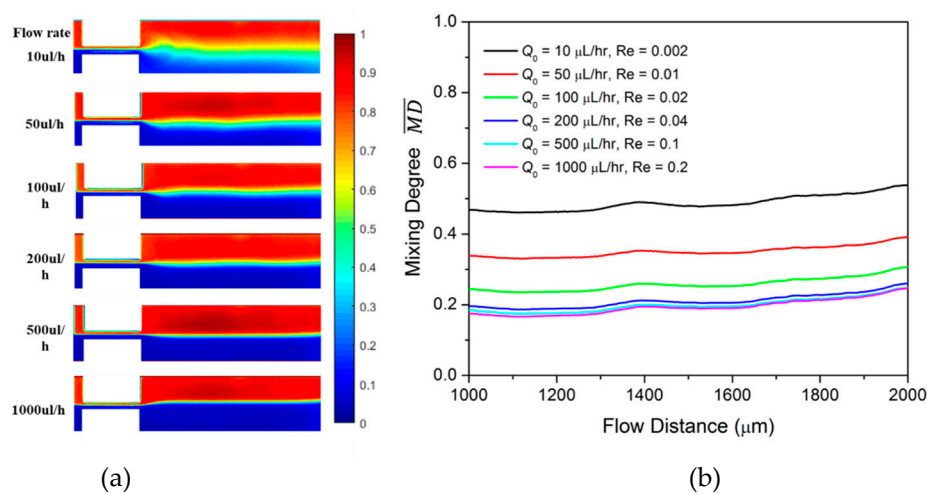

(a) (b)

Figure 2. (**a**) Concentration profile of Newtonian fluid at different constant flow rates; (**b**) the averaged mixing degree $\overline{MD}$ at different constant flow rate mixing.

Then, we modulate fluid A at a time pulsing frequency $f = 0.1$ Hz, 0.2 Hz, and 1 Hz as expressed in Equation (1a) while keeping a constant flow rate of Q_0 for fluid B. It is worth noting that the flow rate remains constant when $f = 0$. The time-averaged mixing degree $\overline{MD}$ from S_1 to S_2 is plotted in Figure 3a–f for different flow rates Q_0. When the fluid is at the low flow rate of 10 μL/h, $\overline{MD}$ is highest at $f = 0$ and gradually decreases as f increases to 1 Hz. A similar trend is also observed for the case when $Q_0 = 50$ μL/h. As discussed previously, the mixing largely relies on the diffusion mechanism in the low flow rate regime; we conclude that the diffusion in the microfluidic channel is affected when the disturbing frequency increases at this low flow rate.

In a higher flow rate of $Q_0 = 100$ μL/h, the $\overline{MD}$ is generally lower compared to that at $Q_0 = 50$ μL/h. However, it remains almost the same when the flow rate increases from $Q_0 = 100$ μL/h to $Q_0 = 200$ μL/h, indicating a similar diffusion impact at the two flow rates. Meanwhile, when $Q_0 = 200$ μL/h, $\overline{MD}$ at $f = 0$ is the lowest compared to that at non-zero pulsing frequencies. This indicates that the disturbance starts to contribute to the diffusion.

As Q_0 increases from 200 μL/h to 500 μL/h, as shown in Figure 3d,e, interestingly, $\overline{MD}$ starts to increase for both $f = 0.1$ Hz and $f = 0.2$ Hz, while it remains about the same for $f = 0$ and $f = 1$ Hz. This phenomenon contradicts with the previous analysis that the mixing should be lower at a higher flow rate because of the shorter diffusion time. Here, we conclude that the impact of the intrinsic diffusion change can be neglected at this high flow rate. Instead, the disturbance contributes more significantly to the diffusion, especially at $f = 0.1$ Hz and $f = 0.2$ Hz, which makes the mixing enhanced compared to that at constant injected flow. As Q_0 increases to 1000 μL/h, the mixing pulsed by the non-zero

frequency is larger compared to that at $f = 0$. It is also noticed that at a fixed flow rate, the $\overline{MD}$ is larger when a lower pulsing frequency is used. In every half period, the difference between the two fluids entering the mixing channel, noted as ΔQ, is larger for a lower f. Therefore, a stronger fluid oscillation in the channel can be induced.
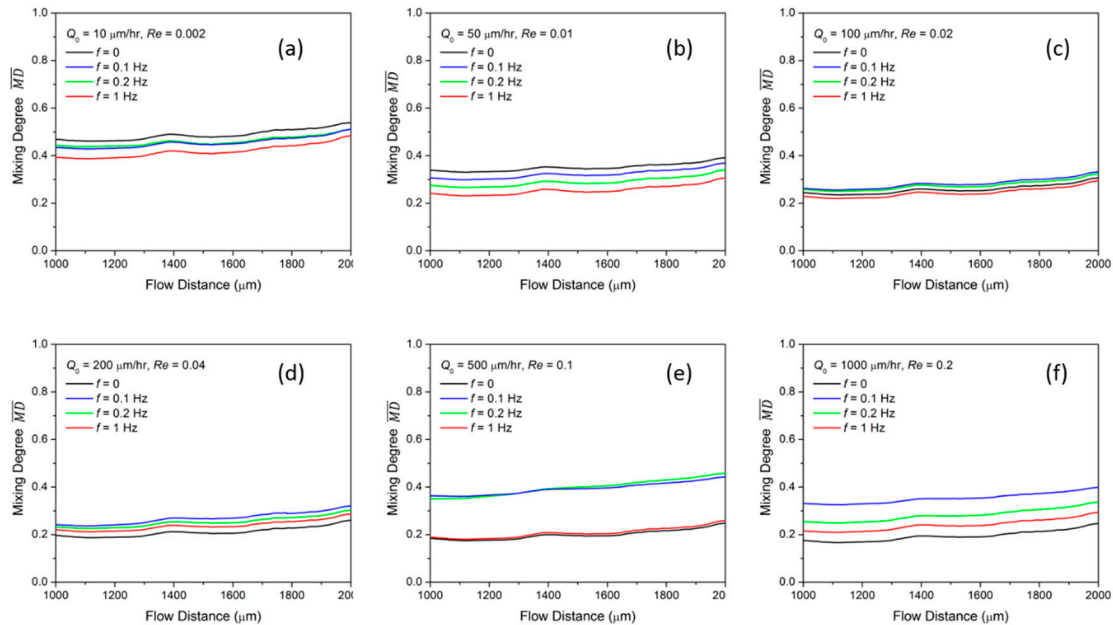

Figure 3. Averaged mixing degree $\overline{MD}$ of time pulsing Newtonian flow with different pulsing frequency at flow rates of (**a**) $Q_0 = 10$ μL/h; (**b**) $Q_0 = 50$ μL/h; (**c**) $Q_0 = 100$ μL/h; (**d**) $Q_0 = 200$ μL/h; (**e**) $Q_0 = 500$ μL/h and (**f**) $Q_0 = 1000$ μL/h.

To further understand the fluid oscillation, we analyze the instantaneous mixing degree MD_t at the flow distance $S_2 = 2000$ μm for 20 s, as shown in Figure 4a–c. For flow rate $Q_0 = 50$ μL/h, the MD_t does not fluctuate for all disturbing frequencies because ΔQ is small at the low flow rate condition. MD_t is highest when $f = 0$, which is due to the high intrinsic diffusion. At flow rate $Q_0 = 200$ μL/h, the MD_t starts to oscillate temporally and the oscillation frequency is identical to the pulsing frequency. Meanwhile, the MD_t for time pulsing is larger than that when $f = 0$. This confirms the contribution of diffusion disturbance to the mixing. At the high flow rate of 500 μL/h, the MD_t oscillates significantly at $f = 0.1$ Hz and 0.2 Hz, which is much higher than that at $f = 0$.

When $Q_0 = 500$ μL/h and $f = 0.1$ Hz (blue line in Figure 4c), MD_t has two peak values A and C and two dip values B and D in each period. The concentration profiles for the peak and dip values are shown in Figure 4d. At the distance S_2, more red fluid oscillates across the center and mixes well with the blue fluid at the peak value A; for peak value C, more blue fluid oscillates across the center and mixes well with the red fluid. For the dip value B, the blue fluid occupies most of the channel and the mixing is low. For the dip value D, both the two fluids occupy half of the channel and little mixing occurs at the center. Therefore, we conclude the enhancement of the mixing for the Newtonian fluid can be induced by the time pulsing flow with a relatively low oscillation frequency.
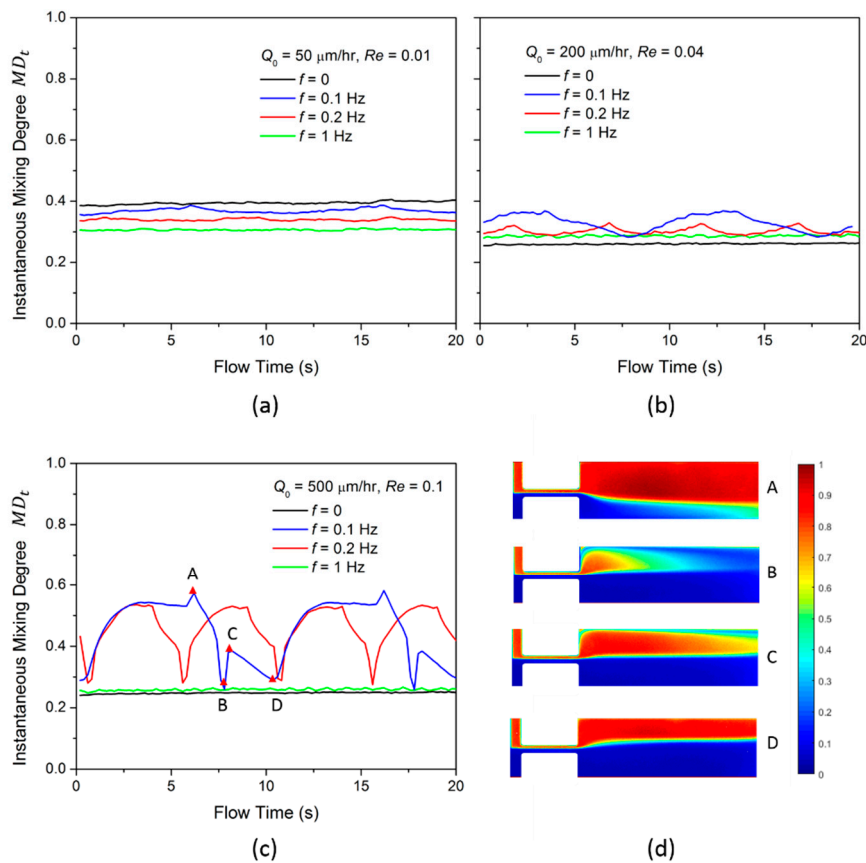
Figure 4. The instantaneous mixing degree MD_t of time pulsing flow with different frequency at flow rates of (**a**) $Q_0 = 50$ μL/h; (**b**) $Q_0 = 200$ μL/h; (**c**) $Q_0 = 500$ μL/h at flow distance 2000 μm; (**d**) the concentration profiles at the peak-value and dip-value time instances when $Q_0 = 500$ μL/h.

3.2. Mixing in Viscoelastic Fluid

The viscoelastic fluid has different rheological properties compared with the Newtonian fluid as it contains elastically stretchable polymers. When injected in the microfluidic T-mixer, the fluid from two inlets will exert stress on each other and, therefore, affect the mixing. In this section, we use the 100 PAM viscoelastic fluid to investigate its mixing behavior. The same injected flow control is applied, as discussed in Section 3.1.

The concentration profiles of the viscoelastic fluid under a constant injection flow rate in the T-mixer are plotted in Figure 5a–f. The flow rate varies from 10 μL/h to 1000 μL/h. The corresponding Weissenberg number *Wi* ranges from 1 to 100. At the low flow rate $Q_0 = 10$ μL/h, the green color fluid occupies most of the channel and indicates good mixing behavior. The corresponding averaged mixing degree $\overline{MD}$ as a function of the flow distance is plotted as the black line in Figure 5g. The red and the blue colored fluids appear on the two sides of the mixing channel at $Q_0 = 50$ μL/h, and the high mixing green regime shrinks to the center area, see Figure 5b, and $\overline{MD}$ lowers as indicated by the red line in Figure 5g. The green mixing area continues to shrink when Q_0 increases from 100 μL/h to 500 μL/h because the diffusion time is decreased for the higher flow rate. Meanwhile, it is noticed that the flow oscillates more significantly at the higher flow rate. As Q_0 increases to 1000 μL/h, the red and the blue fluids are no longer separated on two sides of the channel. Instead, they flow alternatively along the mixing channel, and one fluid pushes the other. It then reaches the channel wall on the other side and rebounds. As can be seen in the pink line in Figure 5g, this largely increases the $\overline{MD}$, which becomes 0.65 at $S_2 = 2000$ μm.

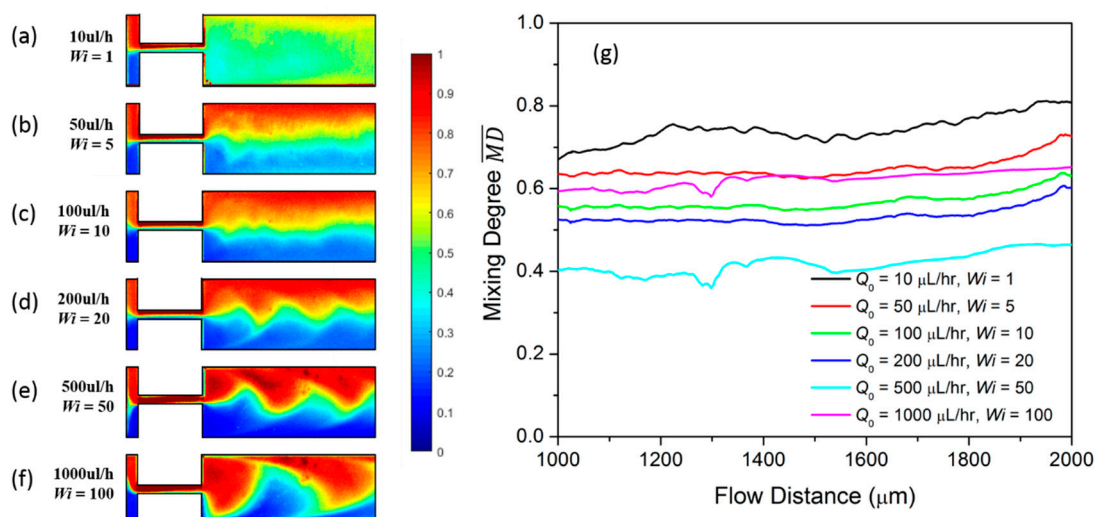**Figure 5.** Concentration profile of viscoelastic fluid at different constant flow rates of (**a**) $Q_0 = 10$ μL/h; (**b**) $Q_0 = 50$ μL/h; (**c**) $Q_0 = 100$ μL/h; (**d**) $Q_0 = 200$ μL/h; (**e**) $Q_0 = 500$ μL/h and (**f**) $Q_0 = 1000$ μL/h; (**g**) the averaged mixing degree $\overline{MD}$ of viscoelastic fluid at different constant flow rates mixing.

Compared with that in glycerol, the mixing degree in PAM is significantly increased. The PAM has similar viscosity to that of glycerol. Therefore, the mixing increase must stem from the non-zero elasticity in PAM. The elasticity of the PAM arises due to the interaction between its molecular structure and the flow. The flow conditions induce a force on the polymers in the fluid, and the polymer chains are stretched and oriented. This nonequilibrium configuration imposes large anisotropic normal stresses, which, in turn, influence the flow field and the mixing effect.

As can be seen in Figure 2a, the concentration contour of glycerol is always symmetric along the whole channel. In addition, the concentration profile in the inlet channel and in the confluence channel are distinctly divided as red and blue colors. While for PAM, as indicated in Figure 5a–f, the concentration contour is not symmetric. In the inlet channel, there is a significant green region between the red color and blue color, indicating the mixing has already started at this point. The mixing in such a narrow area is due to the elastic stress between the two color fluids when they collide with each other. One fluid exerts an elastic force on the other in an alternating fashion, and the two fluids oscillate around the confluence point, which increases the contact area. Specifically, at the low flow rate of $Q_0 = 10$ μL/h, the oscillation amplitude is small and the two fluids flow side by side into the confluence channel. Due to the elastic stress at the confluence point, they continue to mix with each other for a long diffusion time. Therefore, we can observe a significant green region in the narrow confluence channel, which finally results in good mixing in the mixing channel. As indicated in Figure 6, $\overline{MD}$ at $S_2 = 2000$ μm is 0.82. As Q_0 increases to 50 μL/h, 100 μL/h and 200 μL/h, the mixing has a similar mechanism to that when $Q_0 = 10$ μL/h, except that the diffusion time is decreased, thus $\overline{MD}$ decreases gradually. When Q_0 reaches 500 μL/h, the oscillation amplitude is sufficiently high so that the two fluids alternatively enter into the confluence channel; therefore, the mixing in the confluence channel is limited compared to that at a lower flow rate. This explains the large mixing decrease from 0.60 to 0.46 when Q_0 increases from 200 μL/h to 500 μL/h, respectively. As Q_0 increases from 1000 μL/h, the oscillation is so large that the fluids can reach the channel wall on the other side. As explained previously, the fluid will rebound at the wall, which increases the mixing degree.
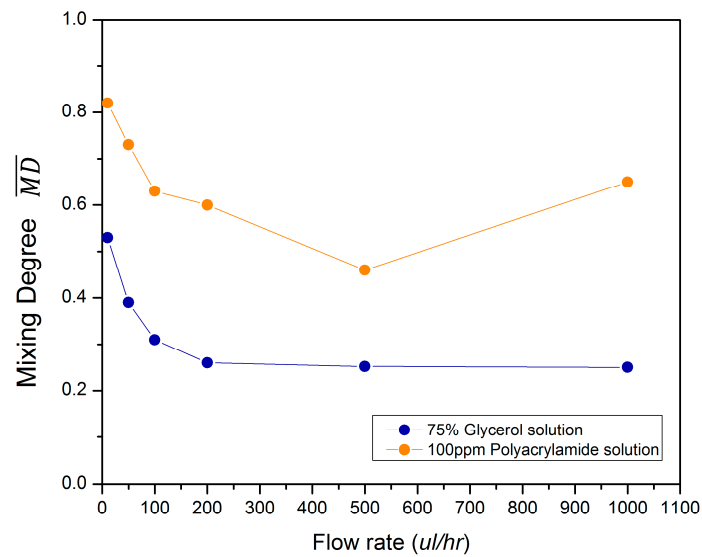
Figure 6. Mixing degree $\overline{MD}$ at S_2 = 2000 μm at different flow rates for both glycerol and polyacrylamide (PAM).

We then investigate the mixing under pulsing flow with the injection condition described in Equation (1). As shown in Figure 7a–d, the $\overline{MD}$ at flow distance S_1 = 600 μm to flow distance S_2 = 2000 μm in the channel is measured for different Q_0, and each sub-figure compares the $\overline{MD}$ modulated at frequency f = 0, 0.1 Hz, 0.2 Hz, and 1 Hz. At a fixed Q_0, lower than 200 μL/h, the $\overline{MD}$ is almost the same for different pulsing frequencies. This means the disturbance from the pulsing does not affect the mixing of the viscoelastic fluid. With Q_0 = 500 μL/h, $\overline{MD}$ is increased from 0.46 to 0.55 at S_2 when the pulsing frequency increases from 0 to 1 Hz, as shown in Figure 7d. To understand the mixing improvement at the non-zero frequency condition, we investigate the instantaneous mixing degree MD_t for a sufficient time in the mixing channel area between S_1 and S_2, as shown in the contour of Figure 8. The x-axis of the contour map is the flow distance and the y-axis is the flow time. It is noticed that some high mixing instances, for example, B, C and D in the contour map of Figure 8b–d, are induced during the flow and contribute to the averaged mixing. Comparably, there is no high mixing region in the constant flow condition and the flow remains almost the same at a relatively low mixing degree, like at point A in Figure 8a. The concentration profiles at points B, C and D are plotted correspondingly and compared with that at point A in the insertion in Figure 8. At point A, the red and blue fluid flow on two sides of the mixing channel and oscillate as a crescent shape due to the elastic stress. While at B, C and D, the flows have similar profiles and the red and the blue fluid flow alternatingly along the channel. This indicates that the oscillation in the constant flow condition is amplified by the time pulsing and results in a higher $\overline{MD}$. As previously discussed in Section 3.1, $\overline{MD}$ is larger at a lower frequency f for the mix in the Newtonian fluid. Here, in contrast, the mixing in the viscoelastic fluid, $\overline{MD}$ is larger at a higher pulsing frequency. The difference of the mixing enhancement between the Newtonian fluid and the viscoelastic fluid stems from the elastic stress in the viscoelastic fluid.
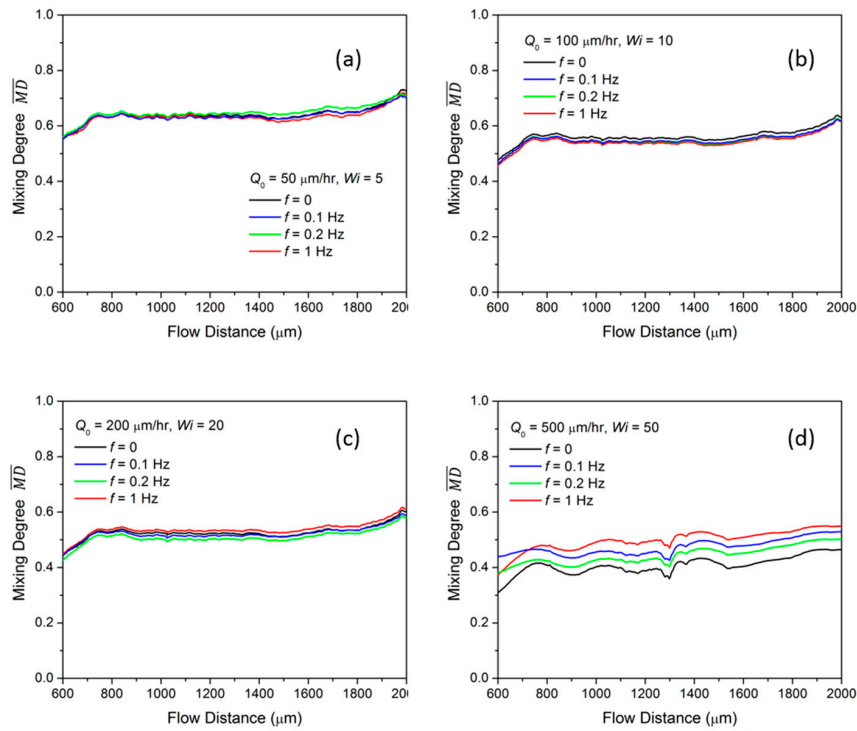
Figure 7. Averaged mixing degree $\overline{MD}$ of time pulsing viscoelastic flow with different frequency at flow rates of (**a**) Q_0 = 50 µL/h; (**b**) Q_0 = 100 µL/h; (**c**) Q_0 = 200 µL/h and (**d**) Q_0 = 500 µL/h.

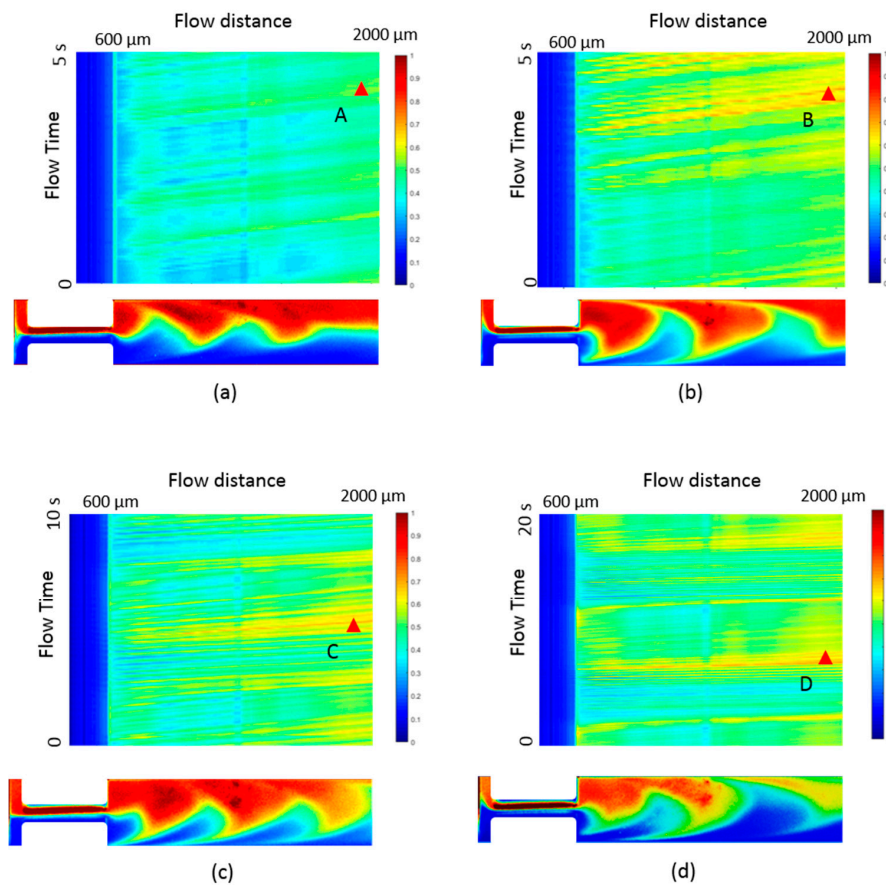**Figure 8.** Top: The instantaneous mixing degree along the flow distance at different flow times with a flow rate of 500 µL/h at a pulsing frequency of (**a**) 0 ; (**b**) 0.1 Hz; (**c**) 0.2 Hz and (**d**) 1 Hz. Bottom: The concentration profiles at the instance of A, B, C, and D, correspondingly.

4. Conclusions

In conclusion: The time pulsed mixing in both the Newtonian fluid and viscoelastic fluid is experimentally investigated in a T-junction micro-mixer. The mixing efficiency of the fluid is compared for different pulsing frequencies and flow rates. In general, the mixing degree in the viscoelastic fluid is higher than that in Newtonian fluid and reaches 0.82 at $Re = 0.002$ and $Wi = 1$ in the micro-mixer. In the Newtonian fluid, compared to that at the constant flow rate, the mixing with time pulsing is decreased when Re is between 0.002 and 0.01, while increased when Re is between 0.1 and 0.2. In the viscoelastic fluid, the time pulsing does not change the mixing degree when $Wi \leq 20$, while it realizes a larger mixing degree at a higher pulsing frequency when $Wi = 50$. The improved mixing in viscoelastic fluid stems from the strong fluid oscillation in the micro-mixer.

References

1.　Yu, C.; Kim, G.B.; Clark, P.M.; Zubkov, L.; Papazoglou, E.S.; Noh, M. A microfabricated quantum dot-linked immuno-diagnostic assay (μQLIDA) with an electrohydrodynamic mixing element. *Sens. Actuators B Chem.* **2015**, *209*, 722–728. [CrossRef]

2.　Kefala, I.N.; Papadopoulos, V.E.; Karpou, G.; Kokkoris, G.; Papadakis, G.; Tserepi, A. A labyrinth split and merge micromixer for bioanalytical applications. *Microfluid. Nanofluid.* **2015**, *19*, 1047–1059. [CrossRef]

3.　Lang, Q.; Ren, Y.; Hobson, D.; Tao, Y.; Hou, L.; Jia, Y.; Hu, Q.; Liu, J.; Zhao, X.; Jiang, H. In-plane microvortices micromixer-based AC electrothermal for testing drug induced death of tumor cells. *Biomicrofluidics* **2016**, *10*, 064102. [CrossRef]

4.　Yeh, S.-I.; Sheen, H.-J.; Yang, J.-T. Chemical reaction and mixing inside a coalesced droplet after a head-on collision. *Microfluid. Nanofluid.* **2015**, *18*, 1355–1363. [CrossRef]

5.　Roberge, D.M.; Ducry, L.; Bieler, N.; Cretton, P.; Zimmermann, B. Microreactor technology: A revolution for the fine chemical and pharmaceutical industries? *Chem. Eng. Technol.* **2005**, *28*, 318–323. [CrossRef]

6.　Microreactors—New Technology for Modern Chemistry Wolfgang Ehrfeld Volker Hessel Holger Löwe Wiley-VCH: Weinheim. 2000. 288 pp. Price £80. ISBN3-527-29590-9. *Org. Proc. Res. Dev.* **2001**, *5*, 89. [CrossRef]

7.　Hessel, V.; Löwe, H.; Schönfeld, F. Micromixers—A review on passive and active mixing principles. *Chem. Eng. Sci.* **2005**, *60*, 2479–2501. [CrossRef]

8.　Abed, W.M.; Whalley, R.D.; Dennis, D.J.C.; Poole, R.J. Experimental investigation of the impact of elastic turbulence on heat transfer in a serpentine channel. *J. Non-Newt. Fluid Mechan.* **2016**, *231*, 68–78. [CrossRef]

9.　Xia, H.M.; Wang, Z.P.; Koh, Y.X.; May, K.T. A microfluidic mixer with self-excited 'turbulent' fluid motion for wide viscosity ratio applications. *Lab Chip* **2010**, *10*, 1712–1716. [CrossRef] [PubMed]

10.　Lemenand, T.; Della Valle, D.; Habchi, C.; Peerhossaini, H. Micro-mixing measurement by chemical probe in homogeneous and isotropic turbulence. *Chem. Eng. J.* **2017**, *314*, 453–465. [CrossRef]

11.　Ward, K.; Fan, Z.H. Mixing in microfluidic devices and enhancement methods. *J. Micromech. Microeng.* **2015**, *25*, 094001. [CrossRef] [PubMed]

12.　Lee, C.-Y.; Chang, C.-L.; Wang, Y.-N.; Fu, L.-M. Microfluidic mixing: A review. *Int. J. Mol. Sci.* **2011**, *12*, 3263–3287. [CrossRef] [PubMed]

13.　Lee, C.Y.; Fu, L.M. Recent advances and applications of micromixers. *Sens. Actuators B Chem.* **2018**, *259*, 677–702. [CrossRef]

14. Cai, G.; Xue, L.; Zhang, H.; Lin, J. A review on micromixers. *Micromachines* **2017**, *8*, 274. [CrossRef] [PubMed]

15. Suh, Y.K.; Kang, S. A review on mixing in microfluidics. *Micromachines* **2010**, *1*, 82–111. [CrossRef]

16. Lee, C.-Y.; Wang, W.-T.; Liu, C.-C.; Fu, L.-M. Passive mixers in microfluidic systems: A review. *Chem. Eng. J.* **2016**, *288*, 146–160. [CrossRef]

17. Buchegger, W.; Wagner, C.; Lendl, B.; Kraft, M.; Vellekoop, M.J. A highly uniform lamination micromixer with wedge shaped inlet channels for time resolved infrared spectroscopy. *Microfluid. Nanofluid.* **2011**, *10*, 889–897. [CrossRef]

18. Tofteberg, T.; Skolimowski, M.; Andreassen, E.; Geschke, O. A novel passive micromixer: Lamination in a planar channel system. *Microfluid. Nanofluid.* **2010**, *8*, 209–215. [CrossRef]

19. Zhang, Y.; Hu, Y.; Wu, H. Design and simulation of passive micromixers based on capillary. *Microfluid. Nanofluid.* **2012**, *13*, 809–818. [CrossRef]

20. Li, L.; Chen, Q.D.; Tsai, C. Three dimensional triangle chaotic micromixer. *Adv. Mater. Res.* **2014**, *875–877*, 1189–1193. [CrossRef]

21. Westerhausen, C.; Schnitzler, L.G.; Wendel, D.; Krzysztoń, R.; Lächelt, U.; Wagner, E.; Rädler, J.O.; Wixforth, A. Controllable acoustic mixing of fluids in microchannels for the fabrication of therapeutic nanoparticles. *Micromachines* **2016**, *7*, 150. [CrossRef] [PubMed]

22. Rife, J.; Bell, M.I.; Horwitz, J.S.; Kabler, M.N.; Auyeung, R.C.Y.; Kim, W.J. Miniature valveless ultrasonic pumps and mixers. *Sens. Actuators A Phys.* **2000**, *86*, 135–140. [CrossRef]

23. Sounart, T.; Baygents, J. Electrically-driven fluid motion in channels with streamwise gradients of the electrical conductivity. *Colloid. Surf. A Physicochem. Eng. Aspect.* **2001**, *195*, 59–75. [CrossRef]

24. El Moctar, A.O.; Aubry, N.; Batton, J. Electro-hydrodynamic micro-fluidic mixer. *Lab Chip* **2003**, *3*, 273–280. [CrossRef] [PubMed]

25. Bau, H.H.; Zhong, J.; Yi, M. A minute magneto hydro dynamic (MHD) mixer. *Sens. Actuators B Chem.* **2001**, *79*, 207–215. [CrossRef]

26. Glasgow, I.; Aubry, N. Enhancement of microfluidic mixing using time pulsing. *Lab Chip* **2003**, *3*, 114–120. [CrossRef] [PubMed]

27. Goullet, A.; Glasgow, I.; Aubry, N. Effects of microchannel geometry on pulsed flow mixing. *Mechan. Res. Commun.* **2006**, *33*, 739–746. [CrossRef]

28. Goullet, A.; Glasgow, I.; Aubry, N. Dynamics of Microfluidic Mixing Using Time Pulsing. Available online: https://www.researchgate.net/profile/Ian_Glasgow/publication/228678991_Dynamics_of_microfluidic_mixing_using_time_pulsing/links/570931c908aed09e916f931c.pdf (accessed on 17 April 2019).

29. Zhang, M.; Cui, Y.; Cai, W.; Wu, Z.; Li, Y.; Li, F.; Zhang, W. High Mixing Efficiency by Modulating Inlet Frequency of Viscoelastic Fluid in Simplified Pore Structure. *Processes* **2018**, *6*, 210. [CrossRef]

30. Glasgow, I.K.; Aubry, N. Mixing Enhancement in Simple Geometry Microchannels. In Proceedings of the ASME 2003 International Mechanical Engineering Congress and Exposition, Washington, DC, USA, 15–21 November 2003; pp. 565–572.

31. Cho, C.-C.; Chen, C.-L.; Tsai, R.-T. A novel microfluidic mixer using aperiodic perturbation flows. *Chem. Eng. Sci.* **2011**, *66*, 6159–6167. [CrossRef]

32. Burghelea, T.; Segre, E.; Bar-Joseph, I.; Groisman, A.; Steinberg, V. Chaotic flow and efficient mixing in a microchannel with a polymer solution. *Phys. Rev. E* **2004**, *69*, 066305. [CrossRef]

33. Pathak, J.A.; Ross, D.; Migler, K.B. Elastic flow instability, curved streamlines, and mixing in microfluidic flows. *Phys. Fluid.* **2004**, *16*, 4028–4034. [CrossRef]

34. Hong, S.O.; Cooper-White, J.J.; Kim, J.M. Inertio-elastic mixing in a straight microchannel with side wells. *Appl. Phys. Lett.* **2016**, *108*, 014103. [CrossRef]

35. Julius, L.A.N.; Jagannadh, V.K.; Michael, I.J.; Srinivasan, R.; Gorthi, S.S. Design and validation of on-chip planar mixer based on advection and viscoelastic effects. *BioChip J.* **2016**, *10*, 16–24. [CrossRef]

36. Grigoriev, R.; Schuster, H.G. *Transport and Mixing in Laminar Flows*; John Wiley & Sons: Hoboken, NJ, USA, 2012.

37. Krishnan, J.M.; Deshpande, A.P.; Sunil Kumar, P.B. *Rheology of Complex Fluids*; Springer: New York, NY, USA, 2010; pp. 3–34.

38. Pakdel, P.; McKinley, G.H. Elastic instability and curved streamlines. *Phys. Rev. Lett.* **1996**, *77*, 2459. [CrossRef]

39. Larson, R.G.; Shaqfeh, E.S.; Muller, S.J. A purely elastic instability in Taylor–Couette flow. *J. Fluid Mechan.* **1990**, *218*, 573–600. [CrossRef]

40. McKinley, G.H.; Pakdel, P.; Öztekin, A. Rheological and geometric scaling of purely elastic flow instabilities. *J. Non-Newtonian Fluid Mechan.* **1996**, *67*, 19–47. [CrossRef]